Vrije Universiteit Brussel

VUB VRIJE
UNIVERSITEIT
BRUSSEL

Preparation and evaluation of mesoporous silica layers on radially elongated pillars

Futagami, Shunta; Hara, T.; Ottevaere, Prof. Dr. Ir. Heidi; Baron, Gino; Desmet, Gert; De Malsche, Wim

Preparation and Evaluation of Mesoporous Silica Layers on Radially Elongated Pillars

Shunta Futagami,[1,2] Takeshi Hara,[1,3] Heidi Ottevaere,[2] Gino V. Baron,[1] Gert Desmet[1] and Wim De Malsche[1]*

[1] Department of Chemical Engineering, Vrije Universiteit Brussel, Pleinlaan 2, 1050 Brussels, Belgium

[2] Department of Applied Physics and Photonics, Brussels Photonics (B-PHOT), Vrije Universiteit Brussel, Pleinlaan 2, 1050 Brussels, Belgium

[3] Division of Metabolomics, Medical Institute of Bioregulation, Kyushu University, 3-1-1 Maidashi, Higashi-ku, Fukuoka 812-8582, Japan

(*) corresponding author

Pleinlaan 2, B-1050, Brussels, Belgium

Tel.: +32 (0) 2 629 3781, Fax.; +32 (0) 2 629 3248, E-mail: wdemalsc@vub.ac.be

Abstract

The present paper describes the application of a sol-gel procedure on radially elongated pillars (REPs) using tetramethoxysilane and methyltrimethoxysilane. After octadecylsilylation, the quality of the porous layered REP (PLREP) columns was evaluated by in-situ determination of migration velocities and band broadening of coumarin dyes with fluorescence microscopy in reversed-phase liquid chromatography. Based on the increase in retention due to the sol-gel process, an increase in accessible specific surface by a factor of 112 was observed. Argon physisorption measurements on bulk monoliths prepared with the same method revealed a predominant pore size of 91 Å. Plate heights as low as 0.4–0.8 µm ($k = 0$–1.97) could be obtained thanks to the very low dispersion of the REP format and to the fact that the applied silica layer was conformally and uniformly deposited on the flow-through channels. A kinetic plot analysis demonstrated that the studied PLREP column will deliver more theoretical plates per unit of time than a packed bed when more than 5.0×10^5 theoretical plates are required.

Keywords

Introduction

Recent advances in the technology of chip-based LC columns are remarkable. Novel particle-packing and retaining techniques have been developed for particulate columns and several organic and inorganic monolithic stationary phases have been introduced [1]. In addition to these particulate and monolithic support structures, also pillar array columns are nowadays used as support structures for chip-based LC columns.

Since the group of Regnier first used perfectly ordered pillars as the stationary-phase support structure in chromatography in 1998 [2], pillar array columns (PACs) have been studied intensively by a limited number of research groups [3–22]. A dramatic reduction of the disorder related eddy dispersion or *A*-term of the van Deemter equation has been consistently demonstrated throughout the past decade, but also the freedom in external porosity, flow-through pore shape and channel depth turned out to be features that can be exploited to further tune and improve the column considerably.

In the early days, PACs were originally used for electro-osmotic flow (EOF) driven separations because of the ease of interfacing for this way of propelling the liquid in the chip, and also because of the extremely promising prospect of the EOF based technique capillary electrochromatography (CEC) at the time. Initial work was mainly conducted using quartz [2,23] and PDMS [24–26], for which the quality of the microfabricated structures was limited compared to what was capable with silicon substrates using Bosch or cryogenic types of deep reactive ion etching [27]. The availability of these ion etching procedures allowing for high aspect ratio (i.e. flow-through width/depth) has been vital for a successful implementation of pressure driven operation, as dispersion has appeared to be extremely sensitive to the (non-)verticality of the support structures.

Recently, it was e.g. demonstrated numerically that a slightly-tapered channel (a deviation of 100 nm in a 8 µm deep channel (spacing 1 µm)) results in a 2.7-fold increase in plate height (non-retained component) compared to a perfectly vertical channel [28].

In order to perform separations of complex mixtures, large plate numbers and therefore also sufficiently long channels are required. To this end, Tsunoda et al. developed pillar-distribution-controlled turns to achieve low-dispersion and low-pressure-drop in the turns in PACs [29]. In parallel, our group introduced the approach with narrow turn channels connected to the wider separation channels with radially elongated pillars (REPs), thereby minimizing peak dispersion, however at the expense of a slightly higher pressure drop [30]. Because the interfacing capillaries are fixed in dedicated etched channels with minimal dead volumes and pressure related forces, pressures of 200–400 bar are generally applied, providing sufficient margin for operation. Both approaches involve the generation of a dedicated turn zone, which has different

71 geometrical characteristics than the main (straight) part of the channel, requiring the control of a local
72 variation in retention.

73 Previous studies of PACs mostly focused on improving column efficiency by optimising the chip designs.
74 Our group introduced the aforementioned REPs and revealed that the REPs led to the reduction of B-term
75 dispersion and an elimination of side-wall effect [21,31,32]. These result in much smaller minimum plate
76 heights of REPs than when using cylinders with the same interpillar distance. It was experimentally and
77 theoretically demonstrated that the column performance of REP columns is equivalent to that of open-
78 tubular (OT) columns with the same flow-through dimension, which are considered as the best possible
79 column format [22,32]. A major advantage of the REP compared to the OT format is however that the
80 volume loadability of the REP column can be 1−3 orders of magnitude larger than that of an OT column,
81 because a REP column can be interpreted as if it were comprised of multiple OT channels in parallel.

82 An important drawback of most studies employing PACs is that the pillars are nonporous, therefore
83 offering only a limited interaction surface. This has as a consequence that the retention capability is limited,
84 and that sample overloading can only be avoided when employing small injection amount with samples at
85 low concentrations (typically 1 nL injection with below 1 mM).

86 To keep the high column efficiency of PACs while increasing the retentive surface on pillars is a
87 challenge, as this additional step can induce structural heterogeneity in the column. To meet such a demand,
88 several approaches have been reported to prepare porous layers on pillars, and those approaches can be
89 divided in top down and bottom up approaches.

90 A prominent top down approach to prepare porous layers in PACs is electrochemical anodization. During
91 the anodization process, porous layers grow inward in the pillars. The resulting anodized structures have a
92 porous silicon layer at the outer portion of the pillar and a nonporous silicon core at the portion. Our group
93 has worked intensively on this technique since the first report of the preparation of the porous layers with
94 anodization in 2007 [33,34], involving variation and fine-tuning of the large number of operational
95 variables that influence the porous layer characteristics. The most relevant parameters are electrolyte type
96 and concentration, doping level of the substrates and applied voltage. This offers an enormous potential for
97 optimization, but has as a drawback that the surface functionalization know-how specific for LC
98 applications is still very limited. It is therefore a formidable task to develop this field given the operational
99 freedom.

100 Bottom up approaches enable creation of porous layers of another material on pillars. Techniques to use
101 carbon nanotubes (CNTs) for PACs have been developed by the group of Kutter [4,5] and the group of
102 Vinet [16,17], and their work has shown that CNTs can be used as a stationary phase in reversed phase

103 CEC and LC. The use of CNTs is quite unique in the field of chromatography, on the other hand, silica, a

104 traditional material in this field, is often selected as the material of the porous layers prepared by bottom up

105 approaches. The group of Sepaniak employed plasma-enhanced chemical vapor deposition (PECVD) of

106 silica [11,12]. PECVD allows for formation of silica layers in open systems. They applied their silica

107 layered columns to pressure-driven LC with reversible sealing as well as ultrathin-layer chromatography in

108 open systems.

109   Another approach to prepare silica layers on pillars is the application of sol-gel deposition. In vessels

110 having high wall to volume ratio, by choosing a proper sol-gel feed solution composition, "surface-directed

111 spinodal decomposition" takes place during the sol-gel transition, and hence single silica layers can be

112 formed on the surface instead of constructing monolithic structure [35]. This approach is similar to the case

113 of preparing porous layers in capillaries [36,37]. Detobel et al. used this technique to prepare mesoporous

114 silica layers on cylindrical pillars [38,39]. They applied a 480 nm thick silica layers on cylindrical pillars

115 of 2.4 µm diameter, 3.2 µm spacing. With a mobile phase of 50% methanol/water (v/v), the C_8-modified

116 porous layered PAC showed a 92 times higher retention factor than a C_8-modified PAC which had the same

117 pillar dimensions but without the silica layers. This increase in retention factor is roughly 3 times larger

118 than the case of anodized pillars with a similar layer thickness, later reported by Callewaert et al. [34].

119 Therefore, the sol-gel processing procedure can be suggested as a promising approach that would be able

120 to combine giving a high column efficiency with enhancing retention ability of PACs.

121   The present study is the first report to prepare porous layers in REP columns, which have a different

122 pillar shape and a flow-through pore shape from PACs with classical cylinders. We applied the

123 aforementioned sol-gel deposition technique using tetramethoxysilane (TMOS) and

124 methyltrimethoxysilane (MTMS), in order to increase retention while maintaining the high column

125 efficiency derived from the pillar shape of REPs. After octadecylsilylation, column performance of porous

126 layered REP columns (PLREPs) was examined by on-chip measurements with four coumarin dyes in

127 reversed-phase LC. The performance of a PLREP column was compared with other format columns with a

128 kinetic plot analysis, showing an attainable separation impedance (E_0) value with a certain theoretical plate

129 number (N) under an operating pressure that is practically available.

130 **Experimental**

131 • Chemicals and Materials.

132   Toluene (HPLC grade, > 99.8%), tetramethoxysilane (TMOS), metyltrimethoxysilane (MTMS), 1 M
133 aqueous acetic acid solution, and polyethylene glycol (PEG) of molecular weight (MW) = 10,000 g/mol
134 were obtained from Sigma-Aldrich Co. (Diegem, Belgium). Octadecyldimethyl-*N*,*N*-dimethylaminosilane
135 was purchased from ChemPur Feinchemikalien and Forschungsbedarf GmbH (Karlsrule, DE). Methanol
136 (LC-MS grade) and acetonitrile (HPLC supra-gradient grade) obtained from Biosolve B.V. (Valkenswaard,
137 NL). Deionized water was produced in-house with a Milli-Q water purification system Merck Millipore
138 (Billerica, MA, USA). Coumarin 440 (C440: 7-amino-4-methyl-2*H*-1-benzopyran-2-one), coumarin 450
139 (C450: 7-(ethylamino)-4,6-dimethyl-2*H*-1-benzopyran-2-one), coumarin 460 (C460: 7-(diethylamino)-4-
140 methyl-2*H*-1-benzopyran-2-one), and coumarin 480 (C480: 2,3,6,7-tetrahydro-9-methyl-1*H*,5*H*,11*H*-
141 [1]benzopyrano-[6,7,8-ij]quinolizin-11-one) were purchased from Vadeno Optical Solutions (Apeldoorn,
142 NL). Coumarins were first dissolved in methanol and then diluted with proper methanol/Milli-Q water
143 mixtures to obtain the concentrations of 0.5 mM, 0.5 mM, 1.0 mM, and 1.0 mM for C440, C450, C460,
144 and C480, respectively in the same solvent as the mobile phase. PTFE filters (0.20 µm × 25 mm) were
145 purchased from Macherey-Nagel (Düren, DE).

146 • Microfabrication

147   A 5.5 cm long and 1 mm wide pillar-array channel (mask design: radially elongated pillars (REPs) with
148 aspect ratio 20 (100 µm in the lateral direction and 5 µm in the axial direction), inter-pillar distance 2.5 µm)
149 was patterned using normal UV photolithography (photoresist, Olin 907-12), followed by a dry etching step
150 (Adixen AMS100DE, Alcatel Vacuum Technology, Culemborg, The Netherlands) to etch the 200 nm thick
151 SiO_2 hard mask underneath. Next, the capillary channels were defined by subsequent mid-UV lithography,
152 etching of the Si layer by a Bosch-type deep-reactive-ion etching step (Adixen AMS100SE) reaching a
153 depth of 115 µm. After this, the resist was removed by oxygen plasma and nitric acid, and the pillars were
154 defined in the SiO_2 mask (also the already defined and partly etched capillary groove was etched further)
155 were subsequently Bosch etched to reach a depth of 15 µm (and the capillary channel a total depth of about
156 130 µm). A diverging flow distributor containing an array of radially stretched diamond-shaped pillars [20]
157 was placed at the capillary-pillar channel interface to ensure a good flow distribution over the entire width
158 of the pillar-array column. The microfluidic channels were subsequently sealed with a Pyrex wafer
159 (thickness 0.5 mm), anodically bonded to the Si substrate using an EVG EV-501 wafer bonder (EV Group
160 Inc., Schaerding, Austria). Then, the chip was diced (100 µm deep) from both sides of the wafer and

161 subsequently cleaved, exposing the channels to insert the interfacing capillaries (108 µm OD and 40 µm

162 ID) into. Then, the capillaries were inserted in the grooves and sealed by epoxy glue.

163 • Preparation of mesoporous silica layers on REPs

164 The mesoporous silica layers in REP columns were produced with a similar protocol to those in fused

165 silica capillaries [37]. A sol-gel feed solution was prepared by adding a mixture of TMOS/MTMS (V_T/V_M

166 = 75/25) to a solution composed of 0.506 g of urea, 5 mL of 0.01 M aqueous acetic acid solution, and 0.250

167 g of PEG with MW = 10,000 g/mol, as previously described for the preparation of hybrid monolithic silica

168 [40]. The feed solution was stirred before filtered with a 0.20 µm filter and charged into a REP column.

169 Hydrothermal treatment for the REP column was carried out at 105° C for 15 h to form mesopores in the

170 silica layers. The obtained PLREP column was then flushed with water to wash out remaining PEG. A

171 silica-bulk rod prepared with the same feed composition were used to characterize the mesoporous structure

172 as described before [37].

173 The C_{18}-modification procedure of the PLREP columns was as follows. First, a PLREP column was

174 flushed with acetonitrile, 50% acetonitrile/toluene (v/v), and then toluene for 3 h each by applying nitrogen

175 gas pressure of 40 bar. C_{18}-modification was carried out with a continuous flow of a mixture of 10%

176 octadecyldimethyl- *N,N*-dimethylaminosilane (ODS-DMA)/toluene (v/v) under 40 bar overnight.

177 Afterwards, the PLREP column was flushed with toluene, 50% acetonitrile/toluene (v/v), and then

178 acetonitrile for 3 h each.

179 • Measurements

180 For chromatographic tests, a LC-20AD instrument (Shimadzu, Kyoto, JP) was used to pump the mobile

181 phase through the REP columns. MXP79800-000 and MXT715-000 (IDEX Health & Science GmbH)

182 valves were controlled by an in-house written C++ program to perform automated sample injection as

183 previously shown in [19]. Fluorescence microscope setup for the on-chip detection consisted of an inverted

184 microscope IX-71 equipped with the U-RFT-T lamp power supply (Olympus, Tokyo, JP), an electron

185 multiplier CCD camera C9100-13 (Hamamatsu Photonics, Shizuoka, JP), a XF1075 387AF28 (wavelength,

186 360−420 nm; Omega Optical Inc., VT, USA) for the excitation filter, and a MF460-80 (wavelength,

187 400−500 nm; Thorlabs Elliptec GmbH, Dortmund, DE) for the emission filter. The fluorescence

188 microscope images were analysed with MatLab R2010a software (Mathworks, MA, USA) to obtain

189 chromatographic data. Peak parking measurements were performed to determine D_{eff} and *B*-term values for

190 each solute, as described earlier in [32].

191   Physical characterization was carried out under the similar conditions as demonstrated in the previous report

192   on porous layered open tube (PLOT) capillary columns [37]. For the scanning electron microscopy (SEM)

193   measurements, pieces of the PLREP columns were produced with pliers, and a thin gold coating was applied

194   using a sputter coater (208 HR, Cressington Scientific instruments Ltd., Watford, UK). SEM images were

195   taken using a field-emission scanning electron microscope JSM-7100F from JEOL Ltd. (Tokyo, JP). In

196   addition, argon physisorption measurements of the corresponding bulk-silica rods were conducted at

197    $-186\,°C$ (87 K) to determine the mesopore size distribution, the mesopore volume, and the specific surface

198   area by applying the non-local density functional theory (NLDFT) [41–43], using an Autosorb-1-MP

199   instrument (Quantachrome corporation, FL, USA).

Results & Discussion

Figure 1 shows SEM images of the prepared silica layers in an 18 µm-deep, 2.5 µm-interpillar distance REP column. The mesoporous silica layer preparation condition employed in this study resulted in the layer thickness of approximately 180 nm, which accordingly gives a flow-through pore dimension of ~2 µm. The layer thickness is almost half the thickness of the porous layers reported by Detobel et al. [39]. It can be assumed that this difference is due to the fact that different silica precursors were used, with the mass difference of the silica precursor in the feed solution as the most relevant parameter, as shown in the earlier study for PLOT column [36]. Also the surface to volume ratio of the structures used in the present study is different from that of the Detobel's work (0.88 µm^2/µm^3 for the former case and 0.40 µm^2/µm^3 for the latter).

The silica layers in the presently studied REP columns were uniformly formed on the silicon substrate (pillars and bottom), however, there were no layers on the glass lid (see SEM images at axial direction in Fig. 1). This is ascribed to the difference in wettability of silicon and glass for the sol-gel feed solution. Despite the wetting difference, the uniformity of the layer thickness can be appreciated from Fig. 1. The cross section of the flow-through pores in REP columns can be considered as a rectangular (the distance between the pillars multiplied by the height of the pillars). Considering there is a negligible volume of porous silica layer on the glass lid, the volumetric phase ratio (*m*) of this column is approximately given by Eq. (1);

$$m = \frac{2d\delta + \delta\,(w - 2\delta)}{dw} \tag{1}$$

wherein *d* is the depth of the channels (18 µm), *w* is the interpillar distance (2.5 µm), and δ is the layer thickness (180 nm). The prepared PLREP column provided a value of *m* = 0.15. This is as large as that of a PLOT column reported by Forster et al. (*m* = 0.15), which had 500 nm thick layer in a 15 µm ID capillary [36], however, smaller than the minimum (*m* = 0.24) of PLOT columns reported by Hara et al. [37]. Further optimization of the sol-gel feed solution composition (increasing the silica precursor amount in the sol-gel feed solution) would result in an increase of the volumetric ratio of PLREP column, as demonstrated for OT capillary columns [37]. However, it should be noted that our present study was dedicated to the fabrication of homogeneous porous-silica layer on the pillars in a REP column with sol-gel processing as a principle task.

Argon physisorption measurements of a bulk-silica rod prepared with the same condition as the silica layers in REP columns were carried out to assess the micro- and mesoposority. This approach was pursued

231   in order to obtain sufficient material for the structural analysis. The argon physisorption isotherm curve

232   obtained for the bulk-silica rod (see Fig. 2A) showed Type IV behavior, which suggests that the material is

233   mesoporous [44]. A cumulative pore volume curve and the pore size distribution were obtained from the

234   NLDFT method (see Fig. 2B). The analysis revealed that the silica material prepared by the present

235   procedure possesses an average pore diameter (D_p) of around 90 Å, a specific pore volume (V_p) of 0.828

236   cc/g, and a surface area of 458 m^2/g, while showing there is no significant micropore volume ($V_p < 0.007$

237   cc/g in the range of $D_p \leq 20$ Å). These values are in quite good agreement with a silica stationary phase

238   used in HPLC for the separation of small molecules with a molecular weight of smaller than 10,000 [45].

239   Thus, it is suggested that our present procedure is adequate to fabricate mesoporous silica layer in REP

240   columns.

241   Fig. 3 shows a chromatogram obtained for four coumarin compounds with column A, which is a C_{18}-

242   modified PLREP column (see experimental section for details). 70% methanol/water (v/v) was applied as

243   mobile phase and fluorescence detection was conducted at 5 cm downstream the injection zone. For C_{18}-

244   modified nonporous REP columns, it was reported earlier that no adequate separation was observed when

245   using a similar mobile phase composition as in the present study [21,31], which is attributed to the much

246   lower specific surface of nonporous pillars. In contrast, a base line separation of the four coumarins was

247   easily achieved using PLREP column A by increasing retentive surface (i.e. porous-silica layer) while

248   maintaining high column efficiency of the REP column. Retention factors $k = 0.60$ (C450), $k = 1.14$ (C460),

249   and $k = 1.97$ (C480) were detected. At linear velocities (u_0) of 1.6 mm/s (far in the C-term regime), plate

250   height values ranged from $H = 1.7$ µm (C440) to $H = 6.1$ µm (C480). Minimal plate height values ranging

251   from $H = 0.4$ µm (C440) to $H = 0.8$ µm (C480) were obtained at an optimal u_0-value (see Fig. 5). These

252   minimal plate height values are still even smaller than those are obtained with nonporous cylinders under

253   an unretained condition ($H = 2.3$ µm (C480) in 100% methanol) [20] due to the REP format and the

254   conformal nature of the applied layers. Comparison of the natural logarithm of the retention factors for

255   C480 with the nonporous REP and PLREP columns, which is plotted as a function of volume fraction of

256   methanol in mobile phase (cf. Fig. 4), allows for an estimation of the increase of the retention ability by the

257   presence of the mesoporous silica layers. The comparison of retention factor for C480 in 60%

258   methanol/water (v/v) shows that the retention is increased by a factor of 112 with the mesoporous silica

259   layers. It is noteworthy that the present PLREP column provides a higher retention gain although the layer

260   thickness is thinner than half of that on cylindrical pillars reported by Detobel et al., where they employed

261   the same comparison procedure [39]. Indeed, when the retention factor for C480 with the prepared PLREP

262   column is compared to that of the Detobel's pillar array column ($k = 1.1$ in 70% methanol/water (v/v)),

263   around 80% increase in the k-value is observed. It is noteworthy that the silica precursor employed in this

264   study was a mixture of TMOS and MTMS, while the silica precursor of Detobel's work was pure TMOS.

The higher retention capacity of the present PLREP column can be attributed to the methyl groups on the silica layer surface derived from MTMS, as was demonstrated for the case of monolithic silica capillary columns [46]. It is evident that the present fabrication procedure for reversed-phase LC with REP column can result in a stronger hydrophobicity for separation.

To demonstrate the reproducibility and the uniformity of the silica-layer-preparation protocol, silica layers in column B was prepared with the same protocol as column A. The on-chip plate height measurements for C440 and C480 were carried out with the C_{18}-modified PLREP columns A and B (see Fig. 5A). In order to assess the uniformity of the deposited layer toward longitudinal direction, plate height values were obtained at 1 cm and at 5 cm (see outline symbols in Fig. 5A), which were indistinguishable within the error of the van Deemter values for each velocity point (relative standard deviation (RSD%) based on 3 values per velocity between 0.1 and 6.8%). The plots of column A and those of column B appeared were also very similar, hinting at a good reproducibility of the sol-gel preparation method.

Fig. 5B shows the plots of plate height against linear velocity for C440, C450, C460, and C480 with column A. In order to accurately determine the B-term, the flow was stopped and the effective diffusion coefficient (D_{eff}) was obtained by plotting the peak variance versus time (during 25 min, with intervals of 5 min, with the shutter closed between the intervals to avoid photobleaching). Peak variances of four coumarins against parking time are shown in Figure S1. The slope of each solute is correlated to $D_{eff,x}$ (x represents the mean flow path) and B-term via Eqs. (2) and (3) [47].

$$\frac{\Delta \sigma_x^2}{\Delta t_{park}} = 2D_{eff,x} \tag{2}$$

$$H_B = \frac{B}{u_0} = \frac{2D_{eff,x}}{u_0}(1+k) \tag{3}$$

The plots in Fig. 5B were fitted with the obtained B-term values (see Table 1) and the van Deemter equation [48].

$$H = A + \frac{B}{u} + Cu \tag{4}$$

293   Reduced van Deemter curves were obtained with $h = H/d_p$, $v = ud_p/D_m$, given by Eq. (5);

294

295
$$h = A' + \frac{B'}{v} + C'v \qquad\qquad (5)$$

296

297   wherein $d_p = 2.14\ \mu m$ (layer-thickness-considered interpillar distance) and D_m values of coumarins in 70%

298   methanol/water (v/v) listed in [37] were used. The calculated non-reduced and reduced van Deemter

299   coefficients are displayed in Table 1. For instance, all the values obtained for non-reduced van Deemter

300   coefficients are significantly lower than those for monolithic silica capillary columns [49], demonstrating

301   that the PLREP column is an appropriate column format to result in high column performance. In addition,

302   the much lower minimal plate heights for PLREP columns (cf. Figs. 6(A) and 6(B)) than what can be

303   expected for OT columns can be explained by the fact that the columns are folded and each axial column

304   segment actually represents additional lateral separation length [32]. When plotting the reduced van

305   Deemter curves of the PLREP columns, the performance can be directly compared with that of OT columns

306   examined under the same measurement conditions.

307   Diffusion coefficient in mobile phase (D_m) and diffusion coefficient in stationary phase (D_s) were

308   obtained with

309

310
$$D_{\mathrm{eff},i} = \tau^2 D_{\mathrm{eff},x} = \frac{D_m + kD_s}{1+k} \qquad\qquad (6)$$

311

312   In Eq. (6), i-coordinate describes the tortuous path followed by the liquid, and $\tau^2 = 9.0$ for REPs with aspect

313   ratio 20 [32]. The calculated D_s values and D_s/D_m values are listed in Table 2. The calculated D_s values are

314   much larger than those obtained in the earlier study with nonporous REPs with the same pillar geometry

315   having a C_8-chain layer instead of the C_{18}-chain layer of the present work [32]. The value of D_s/D_m was

316   equal to 0.07 for the C_8-nonporous REPs, while it is between 0.29 and 0.66 for the present study. The values

317   for the PLREPs are in line with what is typically observed with C_{18}-modified core-shell particles [50,51].

318   As shown in Fig. 7, the separation impedance (E_0), which can be interpreted as a resistance to generating

319   plates, is plotted against plate count (N), accounting for a maximal pressure that can be practically applied.

320   This kinetic plot [52] therefore takes both dispersion and permeability of the systems into account, and

321   allows for identification of which type of separation and sample complexity a column under study can be

322   of interest too. Following Eqs. (7) and (8) give E_0 and N, respectively [52].

323
$$E_0 = \frac{H^2}{K_V} \tag{7}$$

324
$$N = \left(\frac{\Delta P}{\eta}\right)\left[\frac{K_V}{u_0 H}\right]_{exp} \tag{8}$$

325   wherein K_v is the permeability of column A (4.18×10^{-15} m^2, see Fig. S2), ΔP the given pressure drop, and

326   η the viscosity of the mobile phase. The kinetic plots are based on components with a similar retentive

327   behaviour ($k = \sim1$) found in literature [49,53]. The PLREP column produces $N_{opt} = 1.6 \times 10^6$ plates in $t_0 =$

328   230 min. When comparing the PLREP column with a nonporous REP column, the N_{opt} value has shifted

329   from 4.3×10^6 plates (nonporous REP column) to 1.6×10^6 plates (PLREP column). The flow-through pore

330   has been reduced from 2.5 µm to approximately 2.1 µm by growing a 180 nm silica layer, which should

331   shift the optimal condition to shorter column length (a shorter t_0 time). When comparing with the nonporous

332   REP column we see however the reverse. This is due to the stationary phase (C_s) contribution to peak

333   dispersion, as described in Table 2.

334   In comparison of the present PLREP column to an electrochemically anodized cylindrical pillar array

335   column, one can see that the N_{opt} value has decreased from $N_{opt} = 4.8 \times 10^6$ to $N_{opt} = 1.6 \times 10^6$. This is related

336   to the fact that the flow-through pore shape of the REP column, which is mainly a straight channel, is more

337   efficient in producing theoretical plates than that of a cylindrical pillar array column. The average dimension

338   of the flow-through pore is also much small, i.e. 2.1 µm compared to a flow-through pore of 2.5 µm, which

339   leads to reducing column permeability.

340   The pillar array columns mentioned above have been designed with a focus on high efficiency

341   separations and therefore have much large flow-through pores than monolithic and packed bed columns.

342   This results in a positioning of the optimal values of the (N, E_0) curves at much higher N values than for the

343   conventional packed bed and monolithic formats. A 5 µm core-shell particle bed can e.g. not extend above

344    $N = 5.0 \times 10^5$, despite that fact that a pressure of 600 bar has been used here as maximal pressure. With the

345   state-of-the-art monolithic silica capillary column (maximal pressure of 300 bar) [46] plotted in Fig. 7,

346   higher N values are attainable in a shorter t_0 time, but it is kinetically more interesting to use pillar array

347   columns.

348   Also for N values as low as 1.0×10^4 plates the pillar array columns are more performant than the 5 µm

349   packed column. Despite the fact that the flow-through pores of the PLREP and cylindrical pillar array

350   columns should be comparable to a packed column with a particle diameter of 6.3–7.5 µm (using the rule

351 of thumb that the flow-through pore that determines the plate height is roughly 1/3 of the particle diameter),

352 the plate height is much lower. This can be attributed to the lack of Eddy dispersion in the pillar array

353 columns.

354   While for some dedicated application involving well-known samples (with sample components of

355 similar concentrations), or large (bio-)molecules that should not get trapped in a pores matrix (as e.g. ion-

356 pair reversed phase chromatography if nucleotides), one will in practice often choose for a higher

357 concentration loadability and a slightly lower intrinsic performance. Hara et al. have recently produced and

358 characterized porous layered open tube (PLOT) capillary columns of 5 µm diameter have superior kinetic

359 characteristics up to a value of as low as 1.0×10^5 theoretical plates. Despite the superior intrinsic

360 performance of the column, the format is hardly selected because of volume overloading reasons. But there

361 are a number of situations where the PLOT capillary column is the format of choice, as in. e.g. many

362 emerging single cell analysis applications. As discussed in earlier work [22], the REP column can be

363 regarded as a combination of parallel open tubular columns, and therefore has a much higher volume

364 loadability. The REP column is therefore much more versatile in terms of loadability than a PLOT column

365 and seems to have a higher practical potential.

366 **Conclusions**

367   A procedure for sol-gel based mesoporous silica layer deposition in pillar array columns was presented

368 and characterized. SEM measurements demonstrated that the layers have been deposited in a very

369 conformal way. Argon physisorption measurements of a bulk-silica rod suggested that the prepared silica

370 layers were properly mesoporous. The surface area of a REP column increased by the presence of the

371 mesoporous silica layers, e.g., in 60% methanol/water (v/v), the retention factor of a PLREP for C480 was

372 112 times larger than that of a nonporous REP column. The layer uniformity along the column flow

373 direction and the reproducibility of the mesoporous silica layer deposition were confirmed by plate height

374 measurements at two different points and the comparison of the plate height values of two PLREP columns,

375 respectively. The kinetic performance of the PLREP column was superior to other support formats,

376 suggesting the advantage in HPLC separations where high plate numbers are needed.

377

Figure Captions

Fig. 1. Scanning electron micrographs of PLREPs in axial and lateral direction. The porous layer thickness
is approximately 180 nm.

Fig. 2. Pore characterization of a bulk-silica rod by argon physisorption. (A) Isotherm curve, (B) pore size
distribution obtained from NLDFT method.

Fig. 3. Chromatogram obtained for C440, C450, C460, and C480 with an ODS-modified PLREP column.
Detection point: 5 cm downstream from the injection. Mobile phase: 70% methanol/water (v/v). Sample
concentration: 0.5 mM (C440), 0.5 mM (C450), 1.0 mM (C460), 1.0 mM (C480). Measurement
temperature: 25 °C. Linear velocity: $u_0 = 1.6$ mm/s. Plate heights: 1.7 µm (C440), 3.5 µm (C450), 4.5 µm
(C460), 6.1 µm (C480).

Fig. 4. Relationship between natural logarithms of retention factors and mobile phase compositions with
ODS-modified PLREP columns. Symbol: PLREP (red ●), nonporous REP (blue ▲). Solute: coumarin 480.
Measurement temperature: 25 °C.

Fig. 5. Plots of plate height against mobile phase velocity with ODS-modified PLREP columns. Mobile
phase: 70% methanol/water (v/v). Measurement temperature: 25 °C. (A) Comparison of column efficiency
between column A and B. Solute: C440 (●), C480 (◆). Coloured symbols without outline, column A at 5
cm downstream from the injection; Coloured symbols with black outline, column A at 1 cm downstream
from the injection; Open symbols with black outline, column B at 1 cm downstream from the injection. (B)
Plots of four coumarin dyes with column A at 5 cm downstream from the injection. Fitted van Deemter
curves are also shown. Solute: C440 (red ●), C450 (blue ▲), C460 (green ■), C480 (yellow ◆). Detection
point: 5 cm downstream from the injection. Retention factors: $k = 0.60$ (C450), $k = 1.14$ (C460), $k = 1.97$
(C480). Minimal plate height values: $H = 0.4$ µm (C440), $H = 0.6$ µm (C450), $H = 0.5$ µm (C460), $H = 0.8$
µm (C480).

Fig. 6. (A) Plots and fitted curves of reduced plate height against reduced mobile phase velocity obtained
for the PLREP column and a PLOT capillary column [37]. Solute: C440 (red ●), C480 (yellow ◆). (B)
Zoom-in of the plots around the minimums of the curves of the PLREP column. Minimal reduced plate
height values: $h = 0.2$ (C440), $h = 0.4$ (C480).

Fig. 7. Comparison of kinetic performance under a column pressure of 300 bar obtained for the PLREP
column (red) and other support formats: a nonporous REP column (brown) [32], a chemically anodized
cylindrical pillar array column (purple) [34], a particulate column packed with 5 µm particles (orange) [53],

413   a monolithic silica capillary column (blue) [46], and a PLOT capillary column (green) [37]. The column

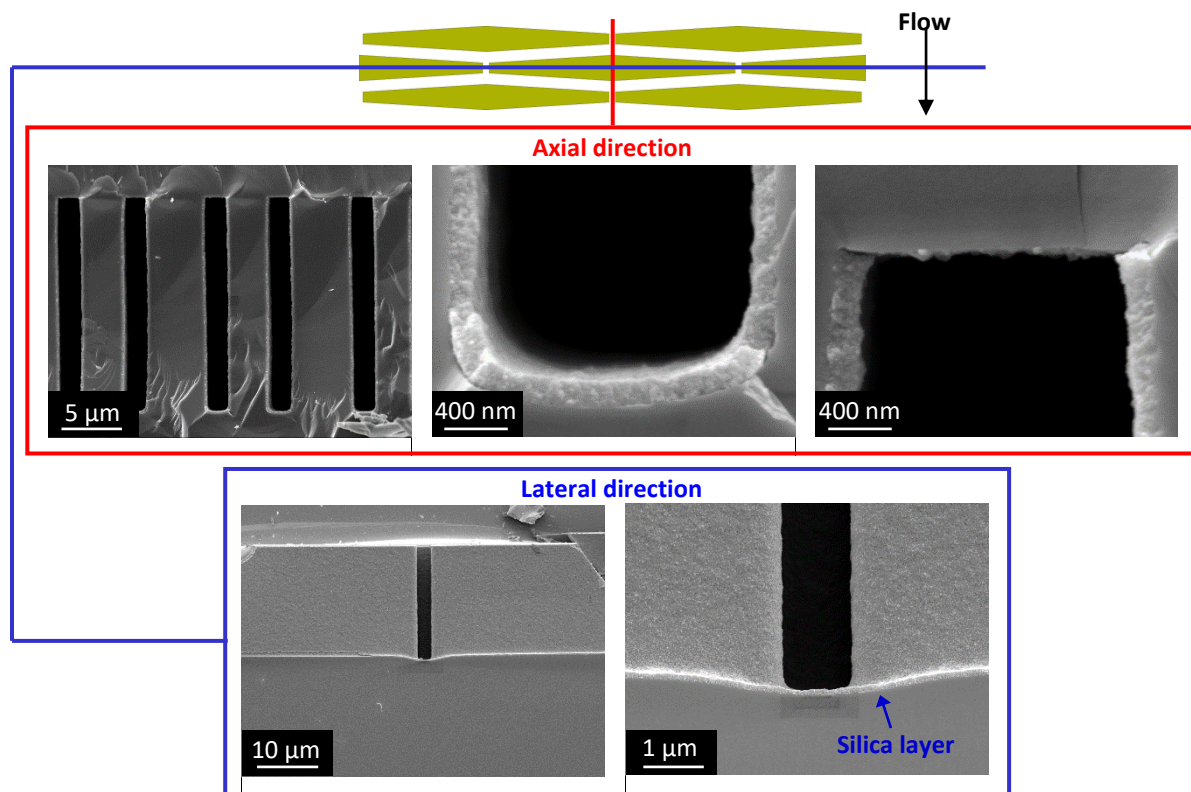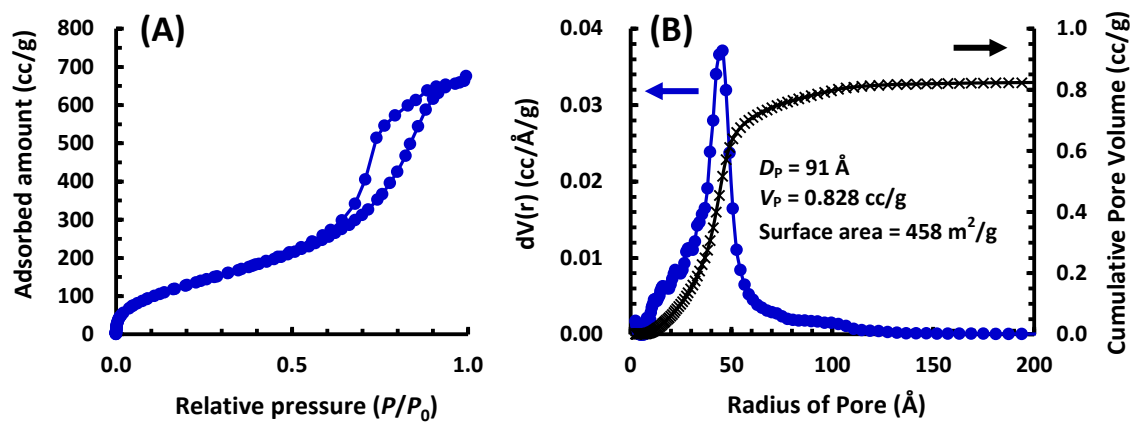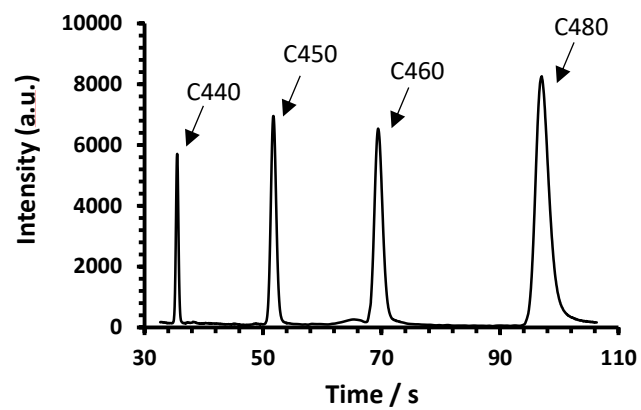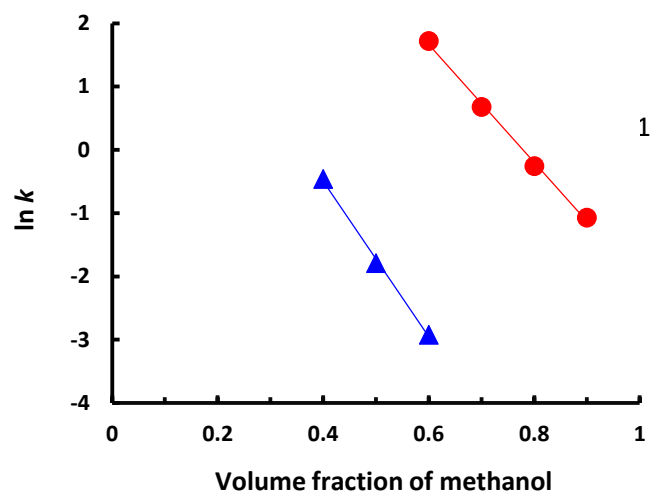414   pressure of the particulate column was exceptionally 600 bar.

415

Fig. 1

416

417

418

419

(A)

(B)

D_P = 91 Å
V_P = 0.828 cc/g
Surface area = 458 m^2/g

420

421

Fig. 2

422

423

424

425

426

427

428

429

430

431

432

433

434

435

436

437

438

Fig. 3

439

440

442

443

444

445

446

447

448

449

450

451

Fig. 4

452
453

455
456
457
458
459
460
461
462
463
464
465
466
467
468
469
470

471

472

Fig. 5

473
474
475
476
477
478
479
480
481
482
483
484
485
486
487
488
489
490
491
492
493
494

Fig. 6

495

496

497

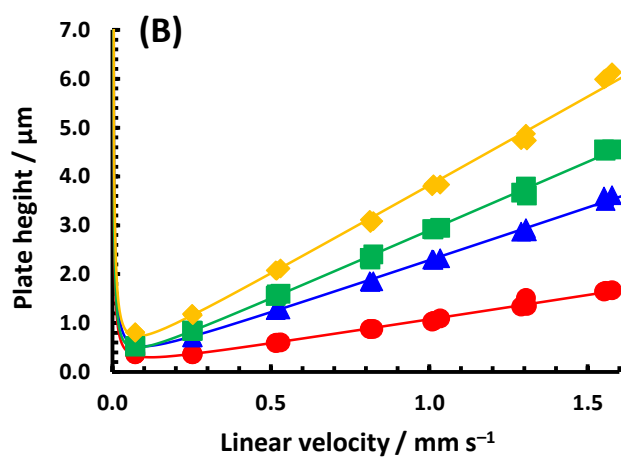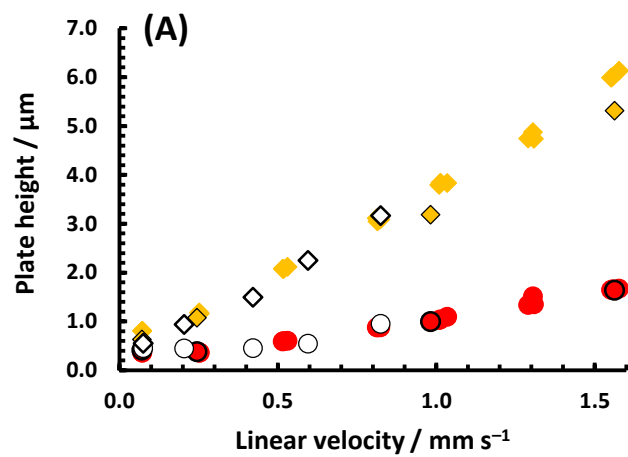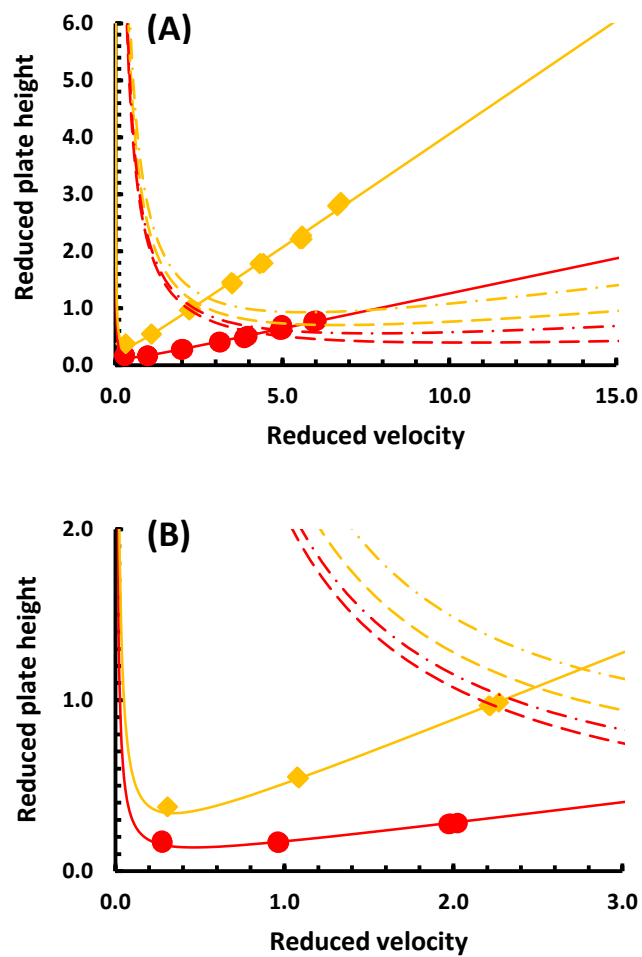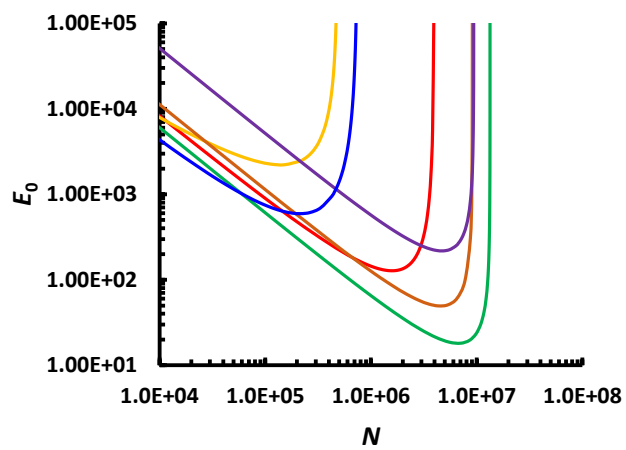498   Fig. 7

499

500   Table 1. Non-reduced and reduced van Deemter coefficients of column A for four coumarins with mobile
501   phase of 70% methanol/water (v/v).

solute	A (m)	B (m^2/s)	C (s)	A'	B'	C'
C440	5.48×10^{-8}	1.48×10^{-11}	1.01×10^{-8}	2.45×10^{-2}	2.65×10^{-2}	1.23×10^{-1}
C450	9.49×10^{-8}	2.12×10^{-11}	2.17×10^{-8}			
C460	6.07×10^{-8}	1.69×10^{-11}	2.82×10^{-8}	2.88×10^{-2}	3.31×10^{-2}	3.14×10^{-1}
C480	1.47×10^{-7}	2.33×10^{-11}	3.65×10^{-8}	6.65×10^{-2}	4.65×10^{-2}	3.99×10^{-1}

502

503

504   Table 2. D_m, D_s and D_s/D_m values for C440, C460 and C480.[a]

solute	D_m (m^2/s)	D_s (m^2/s)	D_s/D_m
C440	5.6×10^{-10}	3.7×10^{-10}	0.66
C460	5.1×10^{-10}	1.5×10^{-10}	0.29
C480	5.0×10^{-10}	2.2×10^{-10}	0.44

505   [a]D_m values in mobile phase of 70% methanol/water (v/v) were taken from [37].

506

References

[1]   J.P. Grinias, R.T. Kennedy, Advances in and prospects of microchip liquid chromatography, Trends Anal. Chem. 81 (2016) 110–117.

[2]   B. He, N. Tait, F. Regnier, Fabrication of nanocolumns for liquid chromatography, Anal. Chem. 70 (1998) 3790–3797.

[3]   O. Gustafsson, K.B. Mogensen, J.P. Kutter, Underivatized cyclic olefin copolymer as substrate material and stationary phase for capillary and microchip electrochromatography, Electrophoresis. 29 (2008) 3145–3152.

[4]   K.B. Mogensen, L. Gangloff, P. Boggild, K.B.K. Teo, W.I. Milne, J.P. Kutter, Carbon nanotubes integrated in electrically insulated channels for lab-on-a-chip applications, Nanotechnology. 20 (2009) 95503.

[5]   K.B. Mogensen, M. Chen, K. Molhave, P. Boggild, J.P. Kutter, Carbon nanotube based separation columns for high electrical field strengths in microchip electrochromatography, Lab Chip. 11 (2011) 2116–2118.

[6]   C. Aoyama, A. Saeki, M. Noguchi, Y. Shirasaki, S. Shoji, T. Funatsu, J. Mizuno, M. Tsunoda, Use of folded micromachined pillar array column with low-dispersion turns for pressure-driven liquid chromatography, Anal. Chem. 82 (2010) 1420–1426.

[7]   Y. Song, M. Noguchi, K. Takatsuki, T. Sekiguchi, J. Mizuno, T. Funatsu, S. Shoji, M. Tsunoda, Integration of pillar array columns into a gradient elution system for pressure-driven liquid chromatography, Anal. Chem. 84 (2012) 4739–4745.

[8]   Y. Song, K. Takatsuki, M. Isokawa, T. Sekiguchi, J. Mizuno, T. Funatsu, S. Shoji, M. Tsunoda, Fast and quantitative analysis of branched-chain amino acids in biological samples using a pillar array column Amino Acid Analysis, Anal. Bioanal. Chem. 405 (2013) 7993–7999.

[9]   Y. Song, K. Takatsuki, T. Sekiguchi, T. Funatsu, S. Shoji, M. Tsunoda, Rapid quantitative method for the detection of phenylalanine and tyrosine in human plasma using pillar array columns and gradient elution, Amino Acids. 48 (2016) 1731–1735.

[10]   N. V. Lavrik, L.C. Taylor, M.J. Sepaniak, Enclosed pillar arrays integrated on a fluidic platform for on-chip separations and analysis, Lab Chip. 10 (2010) 1086–1094.

[11]   L.C. Taylor, N. V. Lavrik, M.J. Sepaniak, High-aspect-ratio, silicon oxide-enclosed pillar structures in microfluidic liquid chromatography, Anal. Chem. 82 (2010) 9549–9556.

[12]   D.R. Lincoln, N. V. Lavrik, I.I. Kravchenko, M.J. Sepaniak, Retention in Porous Layer Pillar Array Planar Separation Platforms, Anal. Chem. 88 (2016) 8741–8748.

[13]   T.B. Kirchner, R.B. Strickhouser, N.A. Hatab, J.J. Charlton, I.I. Kravchenko, N. V. Lavrik, M.J. Sepaniak, Nanoscale pillar arrays for separations, Analyst. 140 (2015) 3347–3351.

[14]   N.A. Crane, N. V. Lavrik, M.J. Sepaniak, Manipulating the inter pillar gap in pillar array ultra-thin layer planar chromatography platforms, Analyst. 141 (2016) 1239–1245.

[15]   E. Mery, F. Ricoul, N. Sarrut, O. Constantin, G. Delapierre, J. Garin, F. Vinet, A silicon microfluidic chip integrating an ordered micropillar array separation column and a nano-electrospray emitter for LC/MS analysis of peptides, Sensors Actuators, B Chem. 134 (2008) 438–446.

[16]   A. Fonverne, F. Ricoul, C. Demesmay, C. Delattre, A. Fournier, J. Dijon, F. Vinet, In situ

548 synthesized carbon nanotubes as a new nanostructured stationary phase for microfabricated liquid
549 chromatographic column, Sensors Actuators B Chem. 129 (2008) 510–517.

550 [17] A. Fonverne, C. Demesmay, F. Ricoul, E. Rouvire, J. Dijon, F. Vinet, New carbon nanotubes
551 growth process in a closed microfabricated channel for liquid chromatography application,
552 Sensors Actuators, A Phys. 167 (2011) 517–523.

553 [18] L. Sainiemi, T. Nissilä, R. Kostiainen, S. Franssila, R. a. Ketola, A microfabricated micropillar
554 liquid chromatographic chip monolithically integrated with an electrospray ionization tip, Lab
555 Chip. 12 (2012) 325–332.

556 [19] W. De Malsche, H. Eghbali, D. Clicq, J. Vangelooven, H. Gardeniers, G. Desmet, Pressure-driven
557 reverse-phase liquid chromatography separations in ordered nonporous pillar array columns, Anal.
558 Chem. 79 (2007) 5915–5926.

559 [20] W. De Malsche, J. Op De Beeck, S. De Bruyne, H. Gardeniers, G. Desmet, Realization of 1×10^6
560 theoretical plates in liquid chromatography using very long pillar array columns, Anal. Chem. 84
561 (2012) 1214–1219.

562 [21] J. Op De Beeck, M. Callewaert, H. Ottevaere, H. Gardeniers, G. Desmet, W. De Malsche, On the
563 advantages of radially elongated structures in microchip-based liquid chromatography, Anal.
564 Chem. 85 (2013) 5207–5212.

565 [22] G. Desmet, M. Callewaert, H. Ottevaere, W. De Malsche, Merging Open-Tubular and Packed Bed
566 Liquid Chromatography, Anal. Chem. 87 (2015) 7382–7388.

567 [23] B. He, J. Ji, F.E. Regnier, Capillary electrochromatography of peptides in a microfabricated
568 system, J. Chromatogr. A. 853 (1999) 257–262.

569 [24] B.E. Slentz, N.A. Penner, F.E. Regnier, Capillary electrochromatography of peptides on
570 microfabricated poly(dimethylsiloxane) chips modified by cerium(IV)-catalyzed polymerization,
571 J. Chromatogr. A. 948 (2002) 225–233.

572 [25] B.E. Slentz, N.A. Penner, F. Regnier, Geometric effects of collocated monolithic support
573 structures on separation performance in microfabricated systems, J. Sep. Sci. 25 (2002) 1011–
574 1018.

575 [26] B.E. Slentz, N. a. Penner, F.E. Regnier, Protein proteolysis and the multi-dimensional
576 electrochromatographic separation of histidine-containing peptide fragments on a chip, J.
577 Chromatogr. A. 984 (2003) 97–107.

578 [27] B. Wu, A. Kumar, S. Pamarthy, High aspect ratio silicon etch: A review, J. Appl. Phys. 108 (2010)
579 51101.

580 [28] M. Callewaert, W. De Malsche, H. Ottevaere, H. Thienpont, G. Desmet, Assessment and
581 numerical search for minimal Taylor–Aris dispersion in micro-machined channels of nearly
582 rectangular cross-section, J. Chromatogr. A. 1368 (2014) 70–81.

583 [29] M. Isokawa, K. Takatsuki, Y. Song, K. Shih, K. Nakanishi, Z. Xie, D.H. Yoon, T. Sekiguchi, T.
584 Funatsu, S. Shoji, M. Tsunoda, Liquid Chromatography Chip with Low-Dispersion and Low-
585 Pressure-Drop Turn Structure Utilizing a Distribution-Controlled Pillar Array, Anal. Chem. 88
586 (2016) 6485–6491. doi:10.1021/acs.analchem.6b01201.

587 [30] J. Vangelooven, S. Schlautman, F. Detobel, H. Gardeniers, G. Desmet, Experimental optimization
588 of flow distributors for pressure-driven separations and reactions in flat-rectangular
589 microchannels, Anal. Chem. 83 (2011) 467–477.

[31] J. Op De Beeck, M. Callewaert, H. Ottevaere, H. Gardeniers, G. Desmet, W. De Malsche, Suppression of the sidewall effect in pillar array columns with radially elongated pillars, J. Chromatogr. A. 1367 (2014) 118–122.

[32] M. Callewaert, G. Desmet, H. Ottevaere, W. De Malsche, Detailed kinetic performance analysis of micromachined radially elongated pillar array columns for liquid chromatography, J. Chromatogr. A. 1433 (2016) 75–84.

[33] W. De Malsche, D. Clicq, V. Verdoold, P. Gzil, G. Desmet, H. Gardeniers, Integration of porous layers in ordered pillar arrays for liquid chromatography, Lab Chip. 7 (2007) 1705–1711.

[34] M. Callewaert, K. Maeno, S. Sukas, H. Thienpont, H. Ottevaere, H. Gardeniers, W. De, Integration of uniform porous shell layers in very long pillar array columns using electrochemical anodization for liquid chromatography, Analyst. 139 (2014) 618–625.

[35] K. Kanamori, K. Nakanishi, K. Hirao, H. Jinnai, Three-dimensional observation of phase-separated siloxane sol-gel structures in confined spaces using laser scanning confocal microscopy (LSCM), Colloids Surfaces A Physicochem. Eng. Asp. 241 (2004) 215–224.

[36] S. Forster, H. Kolmar, S. Altmaier, Synthesis and characterization of new generation open tubular silica capillaries for liquid chromatography, J. Chromatogr. A. 1265 (2012) 88–94.

[37] T. Hara, S. Futagami, S. Eeltink, W. De Malsche, G. V. Baron, G. Desmet, Very High Efficiency Porous Silica Layer Open-Tubular Capillary Columns Produced via in-Column Sol–Gel Processing, Anal. Chem. 88 (2016) 10158–10166.

[38] F. Detobel, H. Eghbali, S. De Bruyne, H. Terryn, H. Gardeniers, G. Desmet, Effect of the presence of an ordered micro-pillar array on the formation of silica monoliths, J. Chromatogr. A. 1216 (2009) 7360–7367.

[39] F. Detobel, S. De Bruyne, J. Vangelooven, W. De Malsche, T. Aerts, H. Terryn, H. Gardeniers, S. Eeltink, G. Desmet, Fabrication and chromatographic performance of porous-shell pillar-array columns, Anal. Chem. 82 (2010) 7208–7217.

[40] M. Motokawa, H. Kobayashi, N. Ishizuka, H. Minakuchi, K. Nakanishi, H. Jinnai, K. Hosoya, T. Ikegami, N. Tanaka, Monolithic silica columns with various skeleton sizes and through-pore sizes for capillary liquid chromatography, J. Chromatogr. A. 961 (2002) 53–63. doi:10.1016/S0021-9673(02)00133-4.

[41] M. Thommes, R. Skudas, K.K. Unger, D. Lubda, Textural characterization of native and n-alky-bonded silica monoliths by mercury intrusion/extrusion, inverse size exclusion chromatography and nitrogen adsorption, J. Chromatogr. A. 1191 (2008) 57–66.

[42] M. Thommes, Physical adsorption characterization of nanoporous materials, Chemie-Ingenieur-Technik. 82 (2010) 1059–1073.

[43] M. Thommes, K.A. Cychosz, Physical adsorption characterization of nanoporous materials: Progress and challenges, Adsorption. 20 (2014) 233–250.

[44] K.S.W. Sing, D.H. Everett, R. a. W. Haul, L. Moscou, R. a. Pierotti, J. Rouquérol, T. Siemieniewska, Reporting physisorption data for gas/solid systems with special reference to the determination of surface area and porosity, Pure Appl. Chem. 57 (1985) 603–619.

[45] L.R. Snyder, J.J. Kirkland, J.W. Dolan, Introduction to Modern Liquid Chromatography, 3rd ed., John Wiley&Sons, Inc., New York, 2010.

631 [46] T. Hara, S. Makino, Y. Watanabe, T. Ikegami, K. Cabrera, B. Smarsly, N. Tanaka, The
632   performance of hybrid monolithic silica capillary columns prepared by changing feed ratios of
633   tetramethoxysilane and methyltrimethoxysilane, J. Chromatogr. A. 1217 (2010) 89–98.

634 [47] J.H. Knox, H.P. Scott, B and C terms in the Van Deemter equation for liquid chromatography, J.
635   Chromatogr. A. 282 (1983) 297–313.

636 [48] J.J. van Deemter, F.J. Zuiderweg, A. Klinkenberg, Longitudinal diffusion and resistance to mass
637   transfer as causes of nonideality in chromatography, Chem. Eng. Sci. 5 (1956) 271–289.

638 [49] T. Hara, G. Desmet, G. V Baron, H. Minakuchi, S. Eeltink, Effect of polyethylene glycol on pore
639   structure and separation efficiency of silica-based monolithic capillary columns, J. Chromatogr. A.
640   1442 (2016) 42–52.

641 [50] A. Liekens, J. Denayer, G. Desmet, Experimental investigation of the difference in B-term
642   dominated band broadening between fully porous and porous-shell particles for liquid
643   chromatography using the Effective Medium Theory, J. Chromatogr. A. 1218 (2011) 4406–4416.

644 [51] G. Desmet, S. Deridder, Effective medium theory expressions for the effective diffusion in
645   chromatographic beds filled with porous, non-porous and porous-shell particles and cylinders. Part
646   I : Theory, J. Chromatogr. A. 1218 (2011) 32–45.

647 [52] G. Desmet, D. Clicq, P. Gzil, Geometry-independent plate height representation methods for the
648   direct comparison of the kinetic performance of LC supports with a different size or morphology,
649   Anal. Chem. 77 (2005) 4058–4070.

650 [53] S. Fekete, D. Guillarme, Kinetic evaluation of new generation of column packed with 1.3 µm
651   core–shell particles, J. Chromatogr. A. 1308 (2013) 104–113.

652

653

654

655